Polymer 55 (2014) 3614–3627

Contents lists available at ScienceDirect

Polymer

journal homepage: www.elsevier.com/locate/polymer

Microwave exfoliated reduced graphene oxide epoxy nanocomposites for high performance applications

Bindu Sharmila T.K. [a, b, c], Ajalesh B. Nair [b, d], Beena T. Abraham [e], P.M. Sabura Beegum [a], Eby Thomas Thachil [b, *]

[a] Department of Applied Chemistry, Cochin University of Science and Technology, Kochi, 682022 Kerala, India
[b] Department of Polymer Science and Rubber Technology, Cochin University of Science and Technology, Kochi, 682022 Kerala, India
[c] Department of Chemistry, T.M. Jacob Memorial Govt. College Manimalakunnu, Oliyapuram, 686679 Kerala, India
[d] BK21 Plus Haptic Polymer Composite Research Team, Department of Polymer-Nano Science and Technology, Jeonju 561-756, Republic of Korea
[e] Department of Chemistry, S.N.M. College Maliankara, Maliankara, 683516 Kerala, India

ARTICLE INFO

Article history:
Received 11 February 2014
Received in revised form
29 April 2014
Accepted 13 May 2014
Available online 22 May 2014

Keywords:
Graphene
Epoxy resin
Nanocomposites

ABSTRACT

Graphene has captured the attention of scientific community due to recently emerging high performance applications. Hence, studying its reinforcing effects on epoxy resin is a significant step. In this study, microwave exfoliated reduced graphene oxide (MERGO) was prepared from natural graphite for subsequent fabrication of epoxy nanocomposites using triethylenetetramine (TETA) as a curing agent via *in-situ* polymerization. Thermogravimetric analysis (TGA), X-ray diffraction (XRD), Raman spectroscopy, Fourier transform infrared spectroscopy (FTIR), C^{13} NMR spectroscopy, X-ray photoelectron spectroscopy (XPS) and ultraviolet–visible (UV–vis) spectroscopy were employed to confirm the simultaneous reduction and exfoliation of graphene oxide. The reinforcing effect of MERGO on epoxy resin was explored by investigating its static mechanical properties and dynamic mechanical analysis (DMA) at MERGO loadings of 0 to 0.5 phr. The micro-structure of epoxy/MERGO nanocomposites was investigated using scanning electron microscope (SEM), transmission electron microscope (TEM) and XRD techniques. The present work reports an enhancement of 32%, 103% and 85% in tensile, impact and flexural strength respectively of epoxy by the addition of even 0.25 phr MERGO. At this loading elastic and flexural moduli also increased by 10% and 65%, respectively. Single-edge-notch three-point-Bending (SEN-TPB) fracture toughness (K_{IC}) measurements were carried out where a 63% increase was observed by the introduction of 0.25 phr MERGO. The interfacial interactions brought about by graphene also benefited the dynamic mechanical properties to a large extent in the form of a significant enhancement in storage modulus and slightly improved glass transition temperature. Considerable improvements were also detected in dielectric properties. The epoxy nanocomposite also attained an ac conductivity of 10^{-5} S/m and a remarkable increase in dielectric constant. The simple and cost effective way of graphene synthesis for the fabrication of epoxy/MERGO nanocomposites may be extended to the preparation of other MERGO based polymer nanocomposites. This remarkable class of materials has thrown open enormous opportunities for developing conductive adhesives and in microelectronics.

1. Introduction

Carbon nanomaterials have a unique place in nanoscience owing to their exceptional electrical, thermal, chemical and mechanical properties [1]. They have found application in areas as diverse as composite materials, energy storage/conversion, sensors, drug delivery, field emission devices and nanoscale electronic components [2]. Of all the carbon based nanofillers graphene is perhaps the newest and has grabbed wide attention since its discovery in 2004. This can be attributed to its novel electronic properties, absent in thicker carbon films or other carbon nanostructures [3] coupled with its unique mechanical and thermal properties. Graphene, a monolayer of sp^2 hybridized carbon atoms arranged in a two-dimensional honeycomb structure continues to invite the attention of the scientific community and industrial researchers [4]. Moreover it is the thinnest material and also, the strongest material ever subjected to measurement [5].

* Corresponding author. Tel.: +91 (0)484 2575723; fax: +91 (0)484 2577747.
E-mail addresses: bindusharmilatk@gmail.com (B.S. T.K.), ethachil@cusat.ac.in, ethachil@gmail.com (E.T. Thachil).

http://dx.doi.org/10.1016/j.polymer.2014.05.032
0032-3861/

Graphene can be prepared via various techniques [6], of which the most commonly researched route are via graphitic oxide (GO) [7] due to scalability and shows potential for the production of graphene sheets in bulk quantities required for the fabrication of polymer composites. Brodie, Staudemaier, Hummers and Tour group have proposed various methods for the synthesis of graphite oxide from graphite [8–11]. But graphene in its oxidized form is nonconductive and it is sensitive to higher temperature. By removing oxygen containing groups (reducing), it is possible to restore these properties. However the structure and electrical properties of reduced graphene oxide can be never fully restored to that of pristine graphene [12].

Chemical and thermal methods are frequently used to reduce graphitic oxide. Microwave assisted exfoliation is a simple yet versatile method to simultaneously achieve the exfoliation and reduction of graphitic oxide [13]. However, pristine graphene contains rare surface functional moieties and possesses limited dispersibility in solvents, seriously affecting its performance [14]. In contrast to pristine graphene, the graphene from the microwave exfoliation still contains some oxygen containing groups on the sheet surface. Due to the presence of residual functionalities, this material is referred to in this article as microwave exfoliated reduced graphene oxide (MERGO) instead of graphene. These functionalities not only allow good dispersion of graphene in polymer matrix, but also provide active sites to form chemical bonds between the graphene nanosheets and the polymer matrix [15]. The prepared graphene shows more thermal stability than that of graphene oxide precursor while its composites show good dielectric properties too.

Epoxy resins are a class of high performance thermosetting polymers having wide applications in adhesives, composites, laminates, coatings etc. [16]. However, epoxy resins are generally brittle which restrict their applications. Nanocomposite technology offers an interesting yet challenging alternative for the modification of polymer matrix properties. There are innumerable publications concerned with multifunctional epoxy nanocomposites based on layered silicates [17,18], single walled and multi walled carbon nanotubes (SWCNT & MWCNT) [19,20], natural graphite [21], carbon black [22] etc. The use of CNT in nanocomposites has been limited to date by challenges in processing, dispersion and their prohibitively high cost. Functionalized graphene holds great promise as an effective new filler [23] as it offers properties that are equivalent to or better than those of SWCNTs but with the advantages of scale and practicality associated with clay. Gallego et al. have evaluated comparison of filler percolation and mechanical properties in graphene and carbon nanotube filled epoxy nanocomposites and concluded that graphene sheet based epoxy nanocomposites offer a wider range of improvement than MWCNT [24]. Yang et al. investigated the synergistic effects between multigraphene platelets (MGPs) and chemically functionalized multiwalled carbon nanotubes (GD400-MWCNTs) on epoxy thermosets [25]. It was found that Stacking of individual MGPs was effectively inhibited by the introduction of GD 400-MWCNT, which lead to impressive enhancement in mechanical and thermal properties. Moreover, graphene fillers at even very low loadings have the potential to match or exceed the performance of large quantities of traditional composite fillers. The exploitation of this class of materials has lead to an enormous range of applications in hi-tech and microelectronics [26]. Zhaman et al. reported developing epoxy/graphene nanocomposites with enhanced toughness through the surface modification of graphene sheets [27]. Wang et al. found that graphene could enhance the properties of epoxy thermosets on functionalizing with organosilane [28]. Feng et al. have probed the reinforcing effect of graphene on spirocyclic phosphazene based epoxy resin [29] and the studies demonstrated that the incorporation of graphene lead to considerable increase in Tg, mechanical and conductive properties.

In this investigation, we have prepared graphene through microwave exfoliation of graphene oxide which in turn was synthesized from graphite by the method suggested by the Tour group. Various techniques have been employed for monitoring the simultaneous reduction and exfoliation of graphene oxide. The simple, easy and cost effective technique of microwave exfoliation produces functionalized graphene sheets (FGS) which provide superb polymer particle interactions during subsequent fabrication of epoxy nanocomposites. Considerable potential exhibited by graphene based nanocomposites and the promises they hold for future, novel FGS based nanocomposites are constantly being sought. This makes MERGO a prime candidate for developing high performance light weight composites that can be tailored to individual applications. The microwave exfoliated reduced graphene oxide epoxy nanocomposites obtained are mechanically robust with good thermo-mechanical properties and improved electrical properties. The dielectric response of the epoxy nanocomposites studied herein also holds promise for the development of new polymer composites with excellent dielectric properties. For these reasons, the present initiative represents an advance over previous work. No literature regarding fabrication of microwave exfoliated reduced graphene oxide epoxy nanocomposites or their static and dynamic mechanical properties as well as dielectric properties have come to the attention of the authors.

2. Experimental section

2.1. Materials

The matrix used in the present study was epoxy resin Araldite GY 250 based on diglycidyl ether of bisphenol A (DGEBA) (epoxy equivalent 187 g/eq) and triethylenetetramine (TETA) hardener under the commercial name HY 951 and was purchased from Emax Glass Fibre and Accessories Pvt. Ltd., Chennai. Graphite powder, sulfuric acid (H_2SO_4, 98 wt%), phosphoric acid (H_3PO_4, 85 wt%) potassium permanganate ($KMnO_4$), hydrogen peroxide (H_2O_2, 30 Vol%), hydrochloric acid (HCl, 35%), ether and ethanol were used for the preparation of graphene oxide. They were purchased from Sigma Aldrich, Bangalore, India. All the chemicals were used as received without further purification.

2.2. Preparation of epoxy/microwave exfoliated reduced graphene oxide (E/MERGO) nanocomposites

The fabrication strategy of E/MERGO nanocomposites is shown in Scheme 1. The graphite platelets were first exfoliated to form graphene oxide using the improved method of Tour group [11]. In a typical process a 9:1 mixture of concentrated H_2SO_4/H_3PO_4 (360:40 ml) was added to a mixture of graphite (3.0 g, 1 wt equiv) and $KMnO_4$ (18.0 g, 6 wt equiv) producing a slight rise in temperature to 35–40 °C. The reactants were heated to 50 °C and stirred for 12 h. The mixture was cooled to room temperature and poured onto ice (~ 400 ml). 30% H_2O_2 was slowly added into the mixture until the solution turned bright yellow. The resulting yellowish brown mixture was centrifuged and the solid material was then washed in succession with 200 ml of water, 200 ml of 30% HCl and 200 ml of ethanol. After this multiple wash, it was coagulated with 200 ml of ether. The solid graphene oxide (GO) obtained after the evaporation of ether, was vacuum-dried overnight at room temperature. The dried GO powder was exfoliated in a microwave oven (T.D.S, Model MW73BD) at ambient conditions and 700 W for 1 min. Upon microwave irradiation, a large volume expansion of the GO powder, accompanied by 'violent fuming' was observed. As

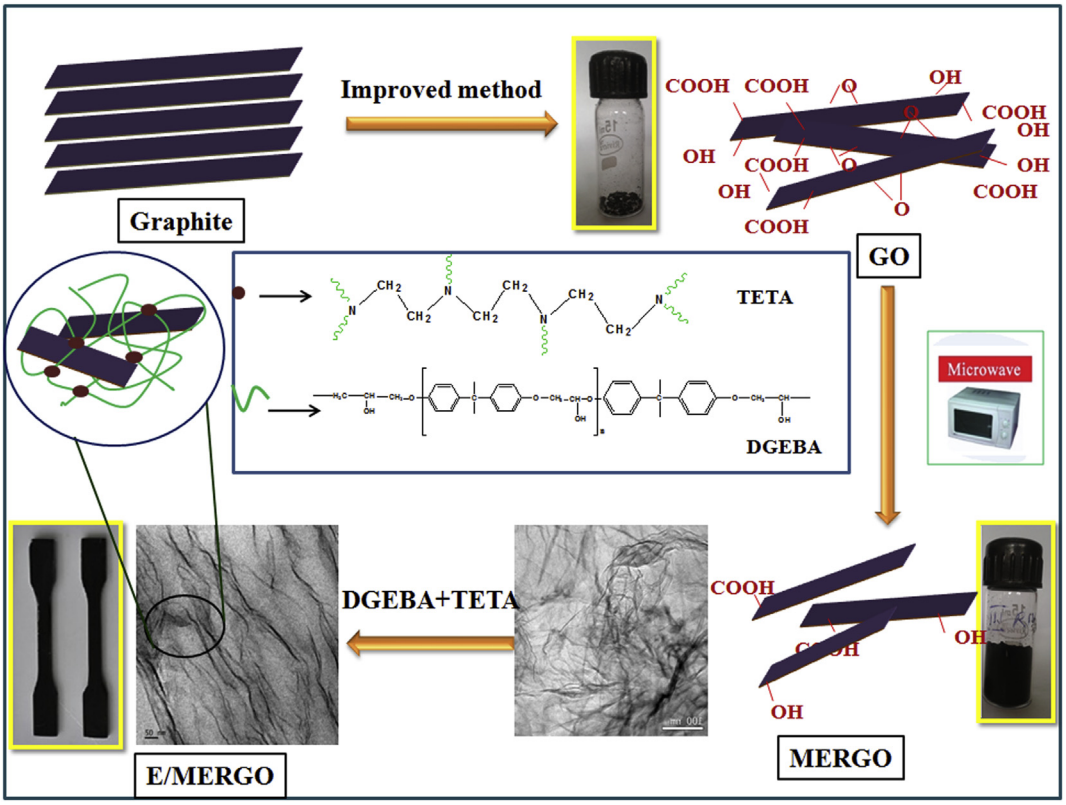

Scheme 1. Fabrication strategy of E/MERGO nanocomposites.

can be seen from Scheme 1, the GO powder in the glass vial had dramatically expanded yielding black and fluffy MERGO.

The epoxy nanocomposite was prepared as follows. First the required quantity of MERGO was dispersed in acetone and it was added to the epoxy oligomer with mechanical stirring for 45 min followed by ultrasonication for another 30 min. The mixture was degassed at 40 °C under vacuum for 30 min to remove the solvent as well as air bubbles. Then 10 phr hardener was added to the epoxy resin, followed by 5 min mixing and degassing. After this, the mixture was transferred into Teflon molds of different shapes coated with a releasing agent and kept for 24 h at room temperature. This was followed by postcuring at 80 °C for 4 h. The cured samples were then demolded and trimmed and used for mechanical studies.

3. Characterization techniques

3.1. X-ray diffraction analysis (XRD)

XRD patterns were employed to portray the graphitic structures of the graphite, GO, and MERGO. The patterns were obtained using a Bruker AXS D8 Advance X-ray powder diffractometer equipped with Cu Kα radiation. The samples were scanned in the range of $2–25^0$ 2θ at increments of 0.020^0 at a wavelength of 1.541 Å operating at 40 KV and 35 mA.

3.2. Raman spectrum

Raman spectroscopy has been utilized as powerful tools for the nondestructive characterization of graphitic structures. It was employed to confirm the structure of GO and MERGO. Raman spectra of GO and MERGO were recorded with Horiba Jobin Yvon Lab Ram HR system at a resolution of 2 mm by using excitation of 514.5 nm of Argon ion laser.

3.3. X-ray photoelectron spectroscopy

X-ray photoelectron spectroscopy (XPS) analysis was carried out on a Kratos Axis Ultra X-ray photoelectron spectroscope (UK) with Al Kα radiation of 1486.6 eV.

3.4. Thermogravimetric analysis

The thermogravimetric analysis of the samples was carried out under nitrogen atmosphere at a heating rate of 20 °C/min in a TGA Q 50 Thermal Analyser (TA Instruments). In all cases the sample weights were between 5 and 10 mg. Thermograms (TG) were recorded for the range from room temperature to 600 °C.

3.5. Fourier transform infrared spectroscopy (FTIR) and UV–visible spectra

Fourier transform infrared spectra (FITR) were recorded on a Jasco FT/IR-4100 instrument. UV–vis spectra were collected on an Evolution 201 UV–visible spectrophotometer. GO dispersion in water and MERGO dispersion in DMF thereafter prepared were diluted to an appropriate absorbance range, and their normalized spectra were compared.

3.6. C^{13} NMR spectroscopy

Solid-state Magic Angle Spinning Nuclear Magnetic Resonance analyses were performed with a 13C HPDEC MAS NMR spectrometer operating at 8 KHz.

3.7. Scanning electron microscopy

SEM observations of graphite, GO, MERGO and the fracture surface of neat epoxy and E/MERGO nanocomposites were examined using a JEOL Model JSM.6390 LV scanning electron microscope. The fracture surfaces were gold coated prior to SEM investigation to make them conductive.

3.8. Transmission electron microscopy (TEM)

The MERGO was dispersed in acetone by ultrasonicator, and some pieces were collected on carbon coated 200 mesh copper grids for TEM observation. For E/MERGO nanocomposite, the ultra thin TEM sample with a thickness of 70 nm was cut using a Leica Ultracut UCT Ultramicrotome at room temperature. Microtomed thin sections were collected on 200 mesh copper grids and examined by a JEM 2100 TEM at 200 kV in a bright field mode.

3.9. Mechanical properties

Tensile properties were tested using a Shimadzu Universal Testing Machine, equipped with a 10 KN load cell at a displacement rate of 5 mm/min at room temperature as per ASTM D 638. The flexural properties were determined using rectangular bars on the same machine, at a speed of 10 mm/min as per ASTM D 790. Impact strength was measured using unnotched samples according to ASTM D 4812-99 on a Ceast Resil Impact analyser (Junior) using a hammer of 4 J at a striking rate of 3.96 m/s. A single-edge-notch three-point-Bending (SEN-TPB) test was conducted to obtain the critical stress intensity factor toughness (K_{IC}) of E/MERGO nanocomposites according to ASTM D 5045 by using the rectangular specimen [See Fig. 6(e)] at a crosshead speed of 10 mm/min. The notches were made first by the formation of saw-cut slots having rectangular shape with a width of ~1 mm in the midsection of specimens. Before testing the specimens were pre-cracked by inserting a fresh razor blade into the sawed notch and impacting with a hammer. The total notch length of SEN-TPB specimen was in such a way that (a/w) should be in between 0.45-0.55, where 'a' is the initial crack length (crack prenotch plus razor tapping notch) and 'w' is the specimen width. Equations (1) and (2) were used to evaluate the fracture toughness of the intrinsically brittle epoxy and E/MERGO nanocomposites by taking 'P' as the critical load for crack propagation and 'B' as the specimen thickness.

$$K_{IC} = \frac{p}{BW^{1/2}} f\left(\frac{a}{w}\right), \quad (x = a/w) \tag{1}$$

$$f\left(\frac{a}{w}\right) = \left\{6x^{1/2}\left[1.99 - x(1-x)\left(2.15 - 3.93x + 2.7x^2\right)\right]\right\} \Big/ \left[(1+2x)(1-x)^{3/2}\right] \tag{2}$$

3.10. Dynamic mechanical analysis (DMA)

The dynamic mechanical thermal analysis was conducted using rectangular test specimens having a dimension of 60 mm × 4 mm × 2 mm with a dual cantilever clamp on a dynamic mechanical analyzer (Model Q 800, TA instruments). The tests were carried out by temperature sweep (temperature ramp from 35 °C to 130 °C at 3 °C/min) method at a constant frequency of 1 Hz to get the dynamic storage modulus (E') and loss modulus (E'') of the samples. Tan δ (E''/E') was calculated as the ratio.

3.11. Dielectric properties and DC electrical conductivity

The dielectric measurements were carried out at frequencies ranging from 20 Hz to 2 MHz using an impedance analyzer, Agilent E 4980 A Precision LCR Meter. Disc shaped samples having diameter 12 mm and thickness 2 mm were used for the measurements. The changes in AC conductivity, real permittivity (ε'), imaginary permittivity (ε'') and dielectric loss tangent (tan δ) of E/MERGO nanocomposites with frequency were obtained from the instrument. The results were directly read on the monitor and recorded on a computer data sheet file. DC electrical conductivity measurements were done by a standard two-probe electrode using a Keithley 2400 source-measure unit in dry air at ambient temperature.

4. Results and discussion

4.1. Structural characterization of MERGO

The XRD pattern of pure graphite, GO and MERGO are shown in Fig. 1(a). Graphite shows a diffraction peak at 26.6^0 corresponding to a basal spacing (d_{002}) of 3.35 Å. The pattern of GO, on the other hand, exhibits a d_{001} reflection at 8.67^0 having a basal spacing of 10.189 Å. Intense intercalation of graphite during oxidation is confirmed by the typical increase of d spacing from 3.35 to 10.189 Å. Nevertheless, the XRD pattern of MERGO does not demonstrate any diffraction peaks due to the disappearance of the long-term ordering graphitic structure.

The major Raman features of graphene and graphite are the so called G band and 2D band. The G band originates from in plane vibration of sp^2 bonded carbon atoms that constitute graphene and is corresponding to the first order scattering of the E_{2g} vibration mode. The 2D band originates from a two phonon double resonance Raman process [30]. A third band known as the defect band (D band) is the result of a one phonon lattice vibrational process. This disorder band is also useful in graphene synthesis as its intensity is directly proportional to the level of defects in the sample [31]. Fig. 1(b) shows the Raman spectra of GO and MERGO. Pure graphite [Fig. 1(b) inset)] exhibits an intense G band at 1580.76 cm^{-1}, 2D band at 2687.99 cm^{-1} and a very weak D band at 1351.9 cm^{-1}. In the Raman spectrum of GO, D band at 1360 cm^{-1} becomes the prominent feature indicating the creation of sp^3 domains or the decrease of sp^2 domains due to extensive oxidation [32]. Additionally, in GO, the G band is broadened and shifted to 1585.42 cm^{-1} owing to the presence of isolated double bonds that resonated slightly at higher frequencies than pure graphite. In MERGO, G band and D band are at 1583.33 cm^{-1} and at 1358 cm^{-1} respectively. Here we got a D/G ratio of 1. Presence of D band and G band confirms the formation of graphene with some defects. This is in agreement with Jingquan et al., who reported that the graphene sheets prepared through oxidation-reduction methods usually retain significant level of defects and possess uncontrolled geometrical shapes due to the harsh oxidation condition [33].

Thermogravimetric and the corresponding differential thermal analysis curves are shown in Fig. 1(c) and (d) respectively. From the TGA curves it is clear that graphite has a good thermal stability on heating up to 900 °C, while GO is thermally unstable and starts to lose mass upon heating below 100 °C. Severe mass reduction at 190 °C is due to the pyrolysis of the labile oxygen containing functional groups, resulting in a rapid thermal expansion of the material. Compared to GO, which has a severe mass reduction at 200 °C [see Fig. 1(d)], MERGO displays a slight reduction in mass. It indicates that oxygen-containing functional groups still remain on the graphene sheets to a small extend after microwave exfoliation.

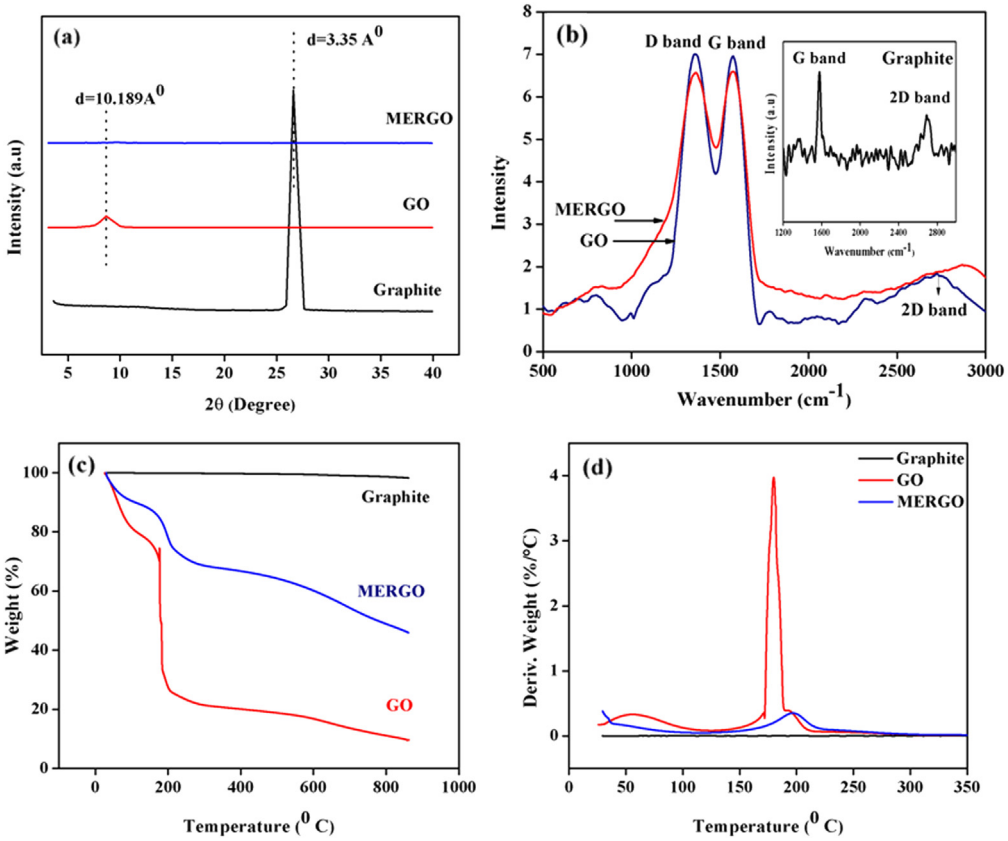

Fig. 1. (a) XRD patterns of pure graphite, GO and MERGO. (b) Raman spectra of,GO & MERGO (inset-Raman spectrum of graphite). (c) TGA and (d) DTG curves of pure graphite, GO and MERGO.

Energy dispersive X-Ray spectroscopy (EDX) analysis of graphite, GO and MERGO are shown in Fig. 2(a,b,c). Only the element carbon (100 atom%) is present in pristine graphite as shown in Fig. 2(a). However, after chemical oxidation, the oxygen concentration drastically increased to 20.05 atom% in GO [Fig. 2(b)]. Compared with spectrum GO, the EDX spectrum of MERGO, [Fig. 2(c)] confirms the reduction process as the elemental oxygen presence decreased to 2.9 atom% with a corresponding increase in atom% of carbon to 97.1.

X-ray photoelectron spectroscopy (XPS) was conducted to investigate the surface elements present, for quantitative analysis and to determine the extent of reduction to graphitic oxide. The corresponding spectra are shown in Fig. 3. Fig. 3(a) shows the wide scan spectra and in both GO and MERGO, C 1s and O 1s signals appear at 286 and 531 eV respectively. Clearly the peaks with binding energies higher than for sp^2 bonded carbon (284.5) are smaller for MERGO [Fig. 3(d)] than for the GO precursor [Fig. 3(c)]. The peaks between 286 and 289 eV are typically assigned to epoxide, hydroxyl and carboxyl groups [34].

The reactive groups of GO and MERGO are also reflected in the FTIR spectra shown in Fig. 4(a). The FTIR spectrum of graphite

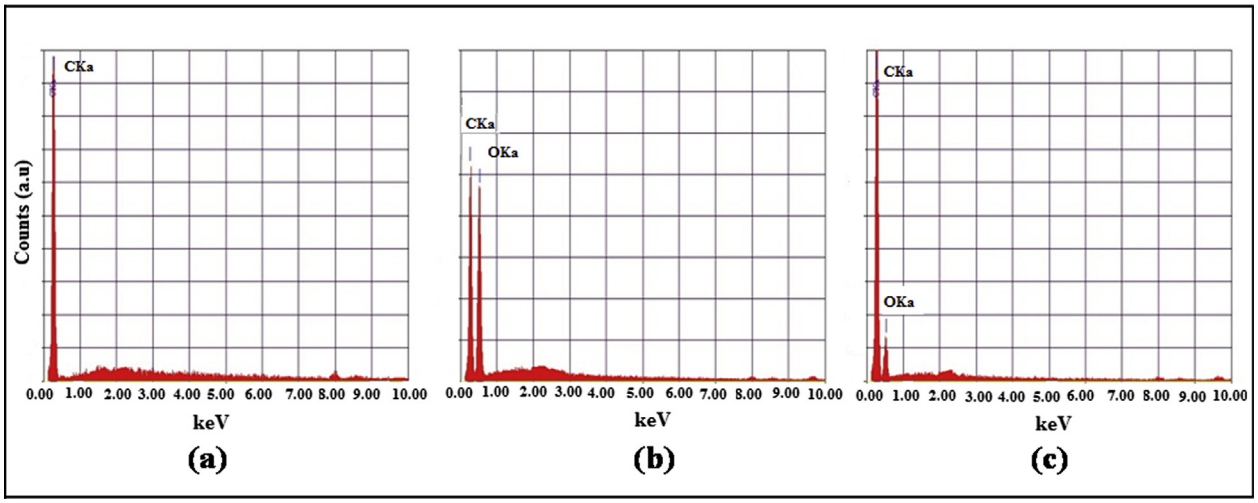

Fig. 2. Energy dispersive X-Ray spectroscopy (EDAX) analysis of (a) graphite, (b) GO and (c) MERGO.

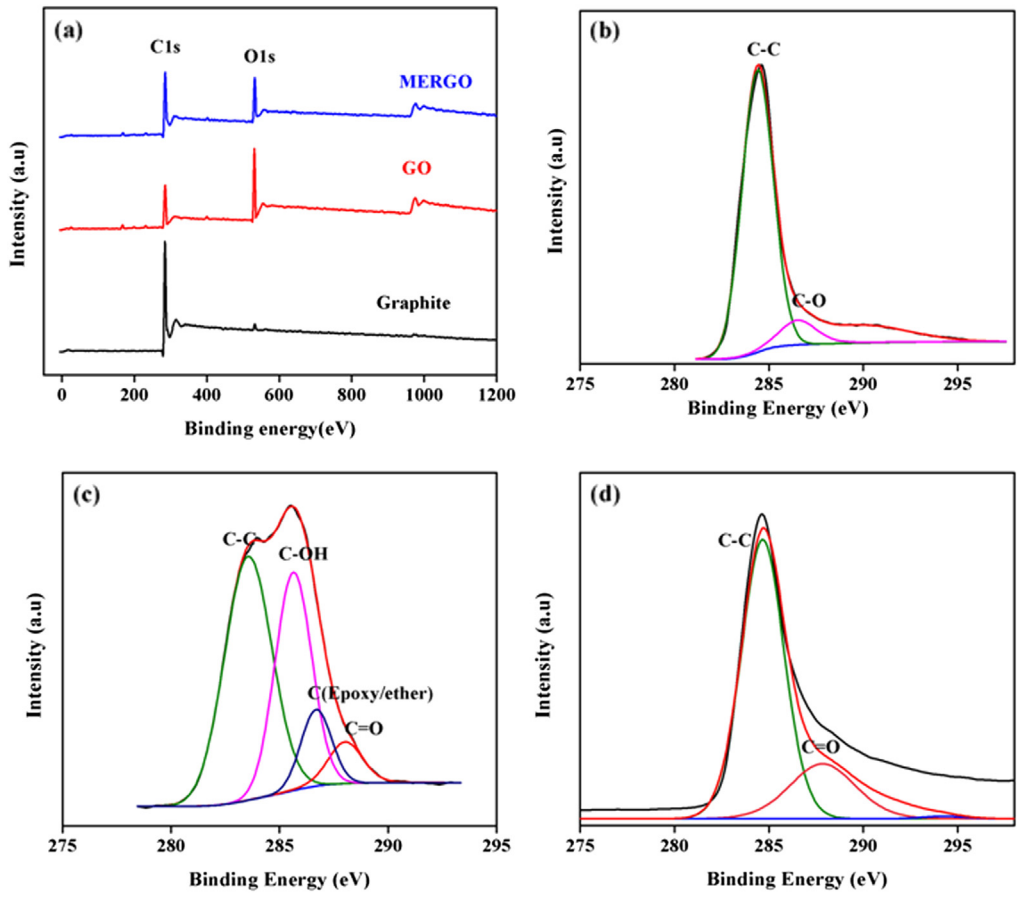

Fig. 3. (a) XPS wide scan spectra. XPS C 1S spectra of (b) Pure graphite, (c) GO and (d) MERGO.

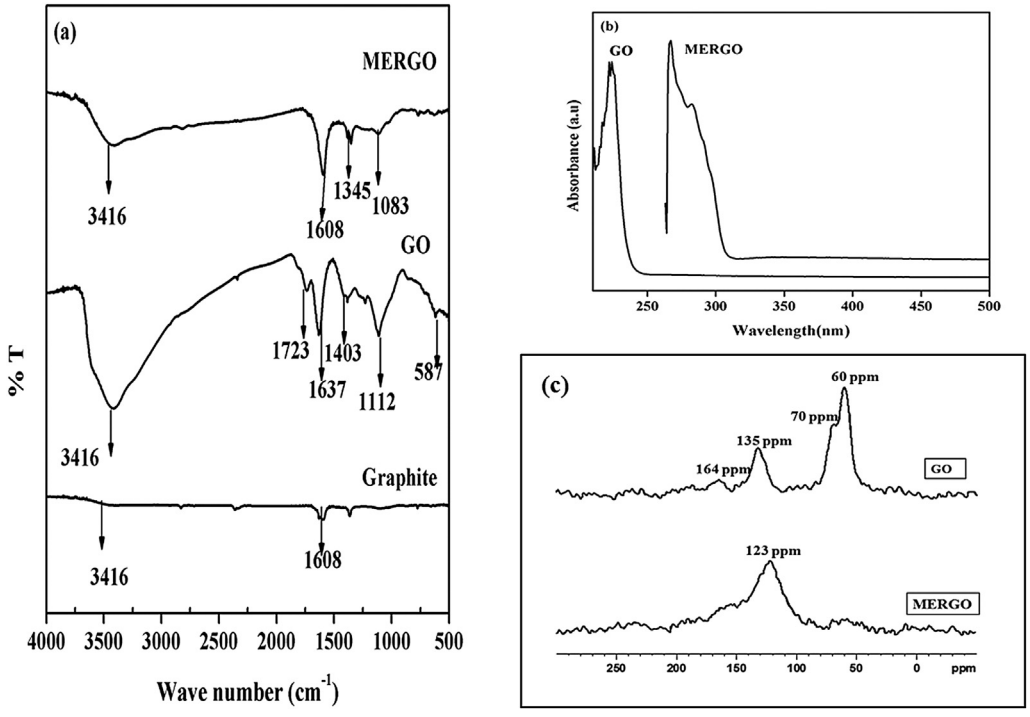

Fig. 4. (a) FTIR spectra of graphite, GO and MERGO, (b) Ultraviolet–visible spectra and (c) C^{13} NMR spectra of GO and MERGO.

shows a vibrational peak of C=C at about 1608 cm^{-1} and a weak shoulder at 3416 cm^{-1}, due to the O–H stretching vibration of the moisture absorbed by the sample. In the case of GO the following functional groups can be identified: O–H stretching vibration at 3416 cm^{-1}, C=O stretching vibration (carbonyl/carboxyl) at 1723 cm^{-1}, from unoxidized sp^2 C=C at 1637 cm^{-1}, a peak at 1403 cm^{-1} assigned to O–H bending deformation or C–O (carboxyl) vibration, and a C–O (alkoxyl) vibration at 1112 cm^{-1}. This confirms the presence of hydroxyl, epoxide, and carbonyl functional groups in GO. However, in MERGO, intensity of O–H stretching vibration at 3416 cm^{-1} gets decreased. C=C stretching at 1608 cm^{-1}, low intensity band at 1396 cm^{-1} assigned to O–H deformations of the C–OH groups and C–O stretching vibrations observed as a very low intensity band at 1083 cm^{-1} are due to the remaining carbonyl groups after the reduction process.

The ultraviolet–visible spectra of GO exhibits a maximum absorption peak at about 223 nm corresponding to π–π^* transition of aromatic C–C bonds. The absorption peak for MERGO had red shifted to 267 nm which indicates that a substantial amount of GO reduction has taken place. This phenomenon of red shift from 223 to 267 nm has been used as a monitoring tool for the reduction of GO or restoration of the conjugated π structure, demonstrated in Fig. 4(b). The weak shoulder around 282 nm in MERGO is attributed to the n–π^* transition of C–O bonds embedded by the exfoliation and intercalation on the reduced graphene oxide.

C^{13} NMR spectroscopy further substantiates the reduction of GO, in agreement with the above results. In C^{13} NMR spectroscopy (See Fig. 4(c) the peaks at 60 and 70 ppm in GO represent epoxide and hydroxyl groups. The peak at 135 ppm corresponds to the presence of unoxidized sp^2 carbon atoms. However in MERGO, the 60 ppm

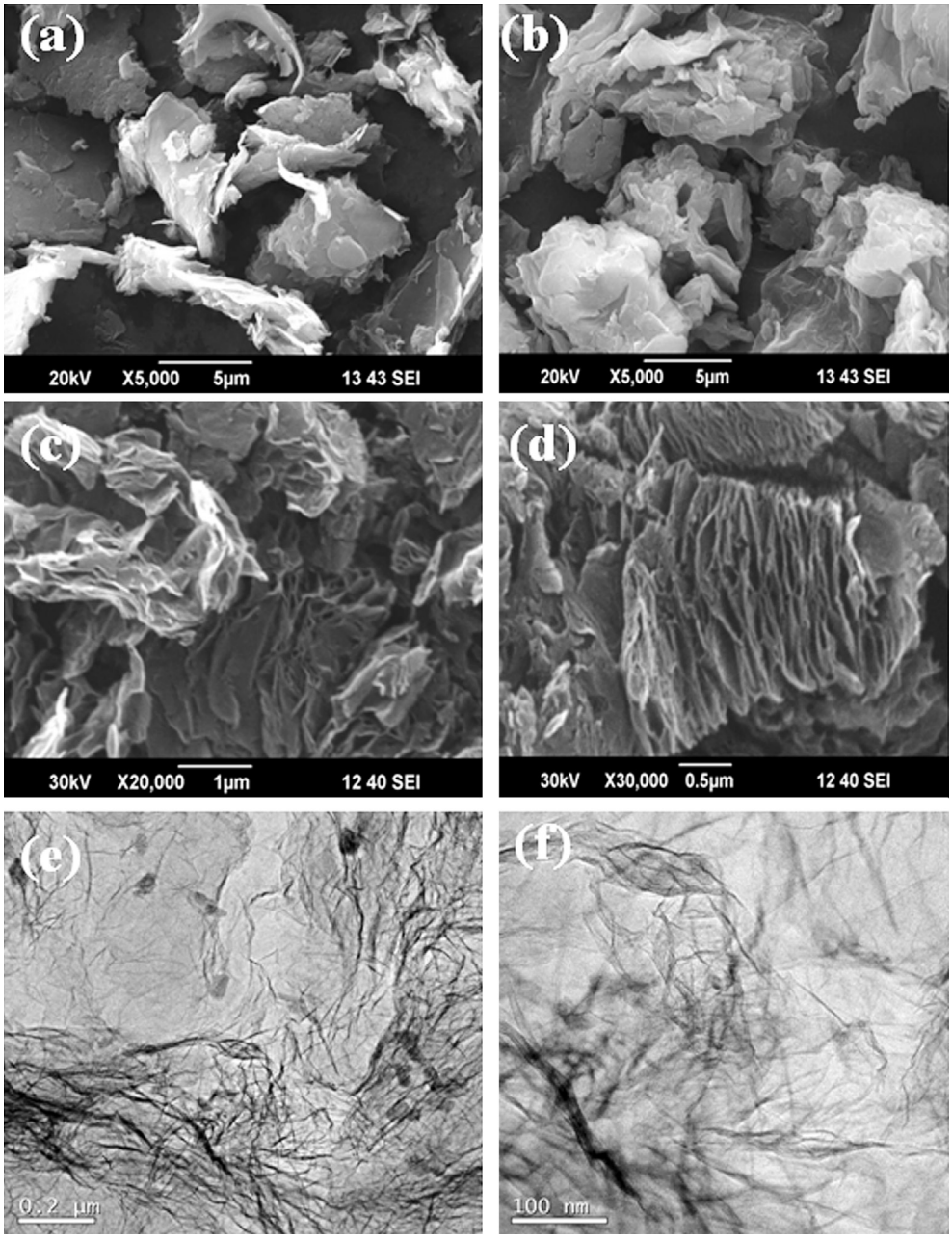

Fig. 5. SEM photograph of (a) graphite, (b) GO, (c) & (d) MERGO, (e) & (f) TEM images of MERGO.

and 70 ppm resonances have disappeared and the peak at 135 ppm shifted to 123 ppm because of the change in the chemical environment of the sp^2 carbon.

Fig. 5(a) and (b) shows the SEM photographs of graphite and GO, which clearly reflect the morphologies of graphite sheets before and after oxidation. The graphite presented a typical multilayer structure whereas the stacking graphitic sheets were separated from one another after oxidation. Fig. 5(b) shows the random orientation and wavy appearance of GO. Fig. 5(c) and (d) represents the higher magnification image of MERGO. It is notable in Fig. 5(c) that the microwave exfoliated reduced graphene oxide exhibits a very small thickness having isolated layers. But in Fig. 5(d), formation of few layer graphene in some areas is also found. It is observed from TEM micrograph of Fig. 5(e and f) that the graphene obtained via microwave exfoliation has wrinkled surface and folds at the edges and has an irregular shape.

4.2. Static mechanical properties of E/MERGO nanocomposites

The influence of MERGO on the mechanical performance of E/MERGO nanocomposites was evaluated in terms of the tensile, flexural and unnotched impact properties. Fig. 6(a) shows the stress–strain curves of neat epoxy and its MERGO nanocomposites. Fig. 6(b), (c) and (d) shows the variation of flexural strength and strain, elastic and flexural moduli and impact strength of the nanocomposites respectively in which the reinforcing effect of the MERGO is clearly brought out.

Examination of these figures leads to the following findings. Tensile, impact and flexural properties present a considerable improvement when MERGO is incorporated into epoxy resin. Such an increasing trend persists with increase of MERGO content till 0.25 phr. At this concentration, the nanocomposite achieved about 32%, 103% and 85% increase in tensile, impact strength and flexural properties respectively, compared to pure epoxy. With the addition of MERGO the strain to failure decreases at higher loading. This is due to the hard and rigid fillers that restrict the elongation and hence the deformation. The E/MERGO nanocomposites exhibit an increasing trend in both elastic and flexural moduli and the highest rate of improvement is obtained at 0.25 phr MERGO loading and thereafter rate of improvement falls until a plateau is reached. The MERGO successfully enhances the interfacial properties upto a 0.25 phr concentration. As MERGO behaves as functionalized graphene, it can form chemical bonds with DGEBA. Epoxy functionalities of MERGO can also react with amine curing agent. Besides

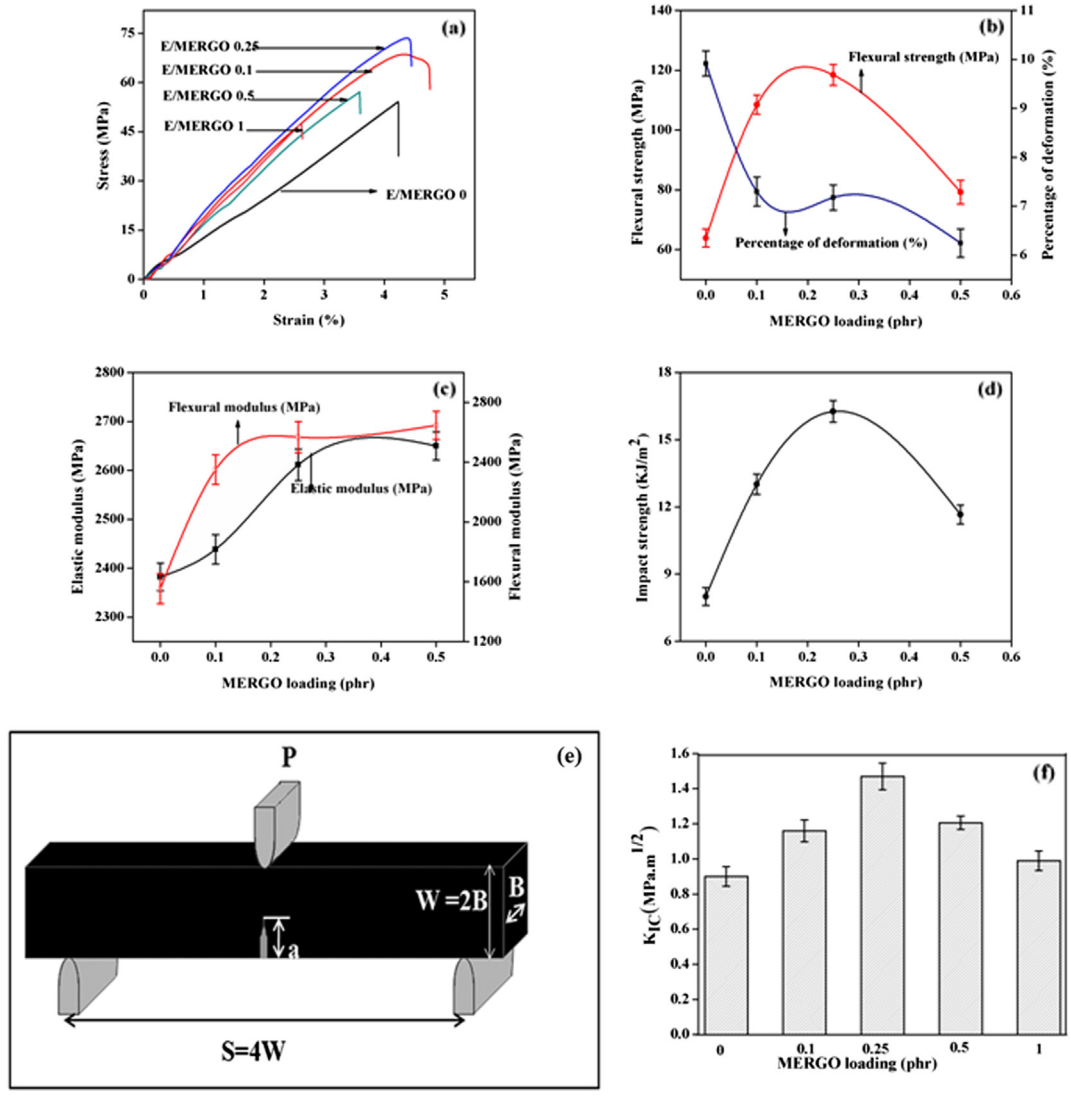

Fig. 6. Mechanical properties of E/MERGO nanocomposites. (a) Stress–strain curves. (b) Flexural strength. (c) Elastic& flexural modulus & (d) Impact strength versus MERGO loadings (phr). (e) Specimen geometry for SEN-TPB fracture toughness test. (f) Fracture toughness against MERGO loading.

chemical interactions, physical cross linking such as hydrogen bonding may also exists in E/MERGO nanocomposites. All the possible interactions are depicted in Scheme 2. In addition, wrinkled topology of MERGO would produce an enhanced mechanical interlocking and adhesion with the epoxy chains and consequently strengthens the interaction and load transfer between MERGO and the epoxy matrix.

When the distribution of the fillers is more homogeneous and no obvious agglomeration is observed, stress transfer between the fillers and the epoxy matrix is more effective [35]. The dispersion of MERGO is good at lower concentrations and at higher values due to excessive interfacial contacts between MERGO/MERGO weakens the mechanical properties of E/MERGO nanocomposites [36]. Moreover the microstructure of E/MERGO nanocomposites may change from fully exfoliated to partially exfoliated/intercalated structure at higher loading and which lead to decrease in mechanical properties as seen in layered polymer nanocomposites. SEM and TEM photographs give credence to the MERGO dispersion in the epoxy matrix, which will be discussed in the coming section.

The SEN-TPB fracture specimens were prepared according to ASTM D 5045 as shown in Fig. 6 (e). Fig. 6 (f) illustrates the effect of the MERGO loading on the fracture toughness of the E/MERGO nanocomposites. The increment in fracture toughness of nanocomposites is believed to be due to the capability of the filler particles to resist the crack propagation before the fracture has taken place. The introduction of 0.25 phr MERGO into the epoxy matrix caused a sharp increase in K_{IC} value (1.47 MPa $m^{1/2} \pm 0.0762$), which corresponds to a 63% increase compared to pure epoxy. The exfoliated kind of dispersion and interfacial interactions are responsible for the improvement in fracture toughness. But as the MERGO loading increases further K_{IC} values decreases. This is because of decrease in the dispersion of the MERGO from exfoliated to partially exfoliated. This will result in the reduction of the resistance of the composite against the crack propagation and subsequently deteriorate the fracture toughness of the composite. In this respect, a decrease in fracture toughness of the composites filled with relatively high MERGO loading is detected. However the K_{IC} value at 1 phr loading is still higher than that of pure epoxy.

4.3. Microstructure of E/MERGO nanocomposites

The SEM image shown in Fig. 7 (a) represents neat epoxy resin, with a relatively smooth surface and occasional river patterns. The resistance of the material under crack propagation is minimal and leads to brittle failure, thus accounting for the low fracture toughness of the unfilled epoxy. Fig. 7(b) and (c) represents the failure surfaces of the nanocomposite containing 0.25 and 0.5 phr of MERGO respectively. Considerable difference is noticed between failure surface of neat epoxy and that of E/MERGO system. On the addition of 0.25 phr of MERGO [Fig. 7(b)] the failure surface becomes rough due to the uniform dispersion of graphene nanosheets in the epoxy matrix. The good compatibility between the nanosheets and the epoxy matrix makes crack propagation difficult and less prone to breakage at this particular loading. From Fig. 7(c), there is clear and irregular entanglement of nanosheets at higher MERGO content.

Morphological investigations of TPB fractured surfaces of pure epoxy and E/MERGO nanocomposites were also inspected by SEM and the corresponding micro photographs are shown in Fig. 7(d)–(i). The characteristic catastrophic brittleness and low fracture toughness of pure epoxy lead to smooth, fragile and mirror like fracture surfaces (Fig. 7(d)). In contrast to the pure epoxy, a rougher surface is observed in Fig. 7(e) indicating that the presence of MERGO forced the crack to propagate along a very tortuous path

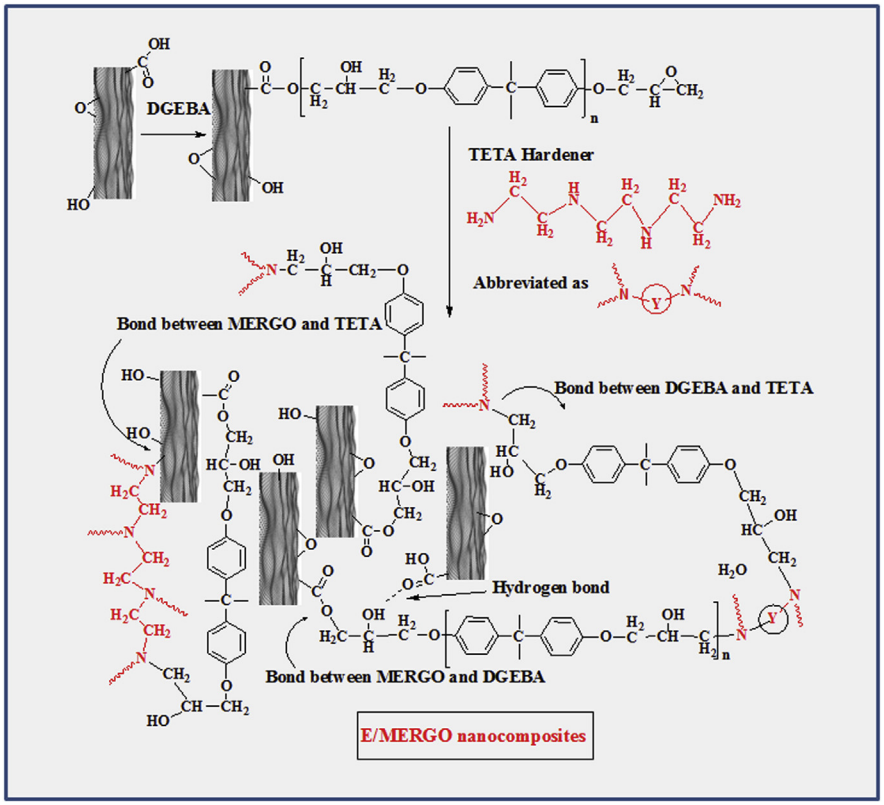

Scheme 2. Schematic illustration of the formation of E/MERGO nanocomposites.

by the creation of matrix plastic deformation and localized shear yielding. Fig. 7 (f) clearly demonstrates the deflection of propagating crack front at 0.25 phr where an initial crack tilted when it encountered a rigid inclusion. This generates an increase in the total fracture surface area resulting in greater energy absorption. The bridge effect, which prevents crack opening, increased strength in the E/MERGO nanocomposites. MERGO sheets are embedded in the matrix and are held tightly by the epoxy resin as depicted in Fig. 7(g). However a dramatic change in morphology is observed at 1 phr loading with much coarser fracture surface [Fig. 7(h)] and its higher magnification image [Fig. 7(i)] shows single graphene or stacks of graphene with thickness of several nanometers protrude out of the fracture surface.

The morphology and the actual pattern of MERGO layer dispersion in the E/MERGO nanocomposites were investigated by TEM to corroborate with mechanical properties. TEM image of E/MERGO nanocomposite with 0.25 phr MERGO loading at different magnifications are shown in Fig. 8(a) and (b) to reveal the dispersion. The dark hair-like structures represent the cross section of the MERGO layers. The MERGO is dispersed well in the epoxy matrix as single or ultra thin sheets of thickness less than several nanometers without the need for additional functionalization. The interfacial interactions brought by the presence of residual epoxy and hydroxyl sites present on the MERGO sheets and the epoxy matrix facilitate the dispersion of graphene nanosheets providing good bonding between MERGO and epoxy, resulting in an exfoliated nanoscale dispersion.

Selected area electron diffraction (SAED) pattern of E/MERGO nanocomposite with 0.25 phr [Fig. 8(c)] shows the amorphous nature of the nanocomposite. The exfoliated kind of dispersion at low loadings of MERGO is also reflected in the XRD analysis as demonstrated in Fig. 8(d). Pure epoxy exhibits a broad peak at 18.5^0, reflecting its amorphous nature. The nanocomposites also possess only this peak and do not exhibit any other peak, which further confirms the effective dispersion of MERGO in the epoxy matrix.

4.4. Dynamic mechanical analysis

Fig. 9(a), (b) and (c) shows the results of DMA tests including storage modulus (E'), loss modulus (E''), and damping factor ($\tan\delta$) as a function of temperature from 35 to 140 °C for the cured pure epoxy and cured E/MERGO nanocomposites at different MERGO

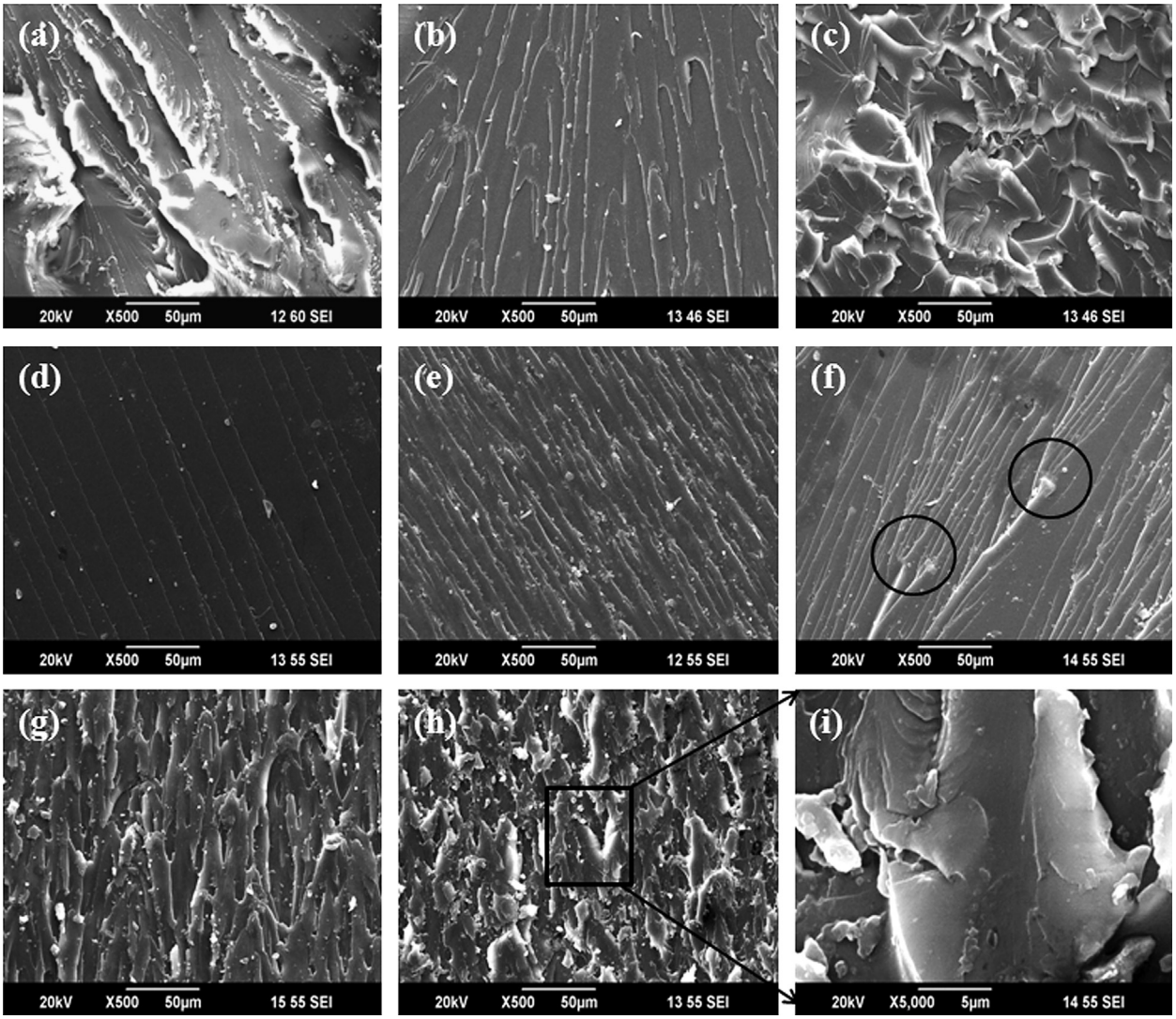

Fig. 7. SEM photographs. (a–c) Fractured surfaces of tensile test specimens of (a) pure epoxy, (b) E/MERGO at 0.25 phr, (c) E/MERGO at 0.5 phr. (d–i) Fractured surfaces of SEN-TPB test specimens of (d) pure epoxy, (e) E/MERGO at 0.1 phr, (f) E/MERGO at 0.25 phr, (g) E/MERGO at 0.5 phr (h & i) E/MERGO at 1 phr nanocomposites.

loadings. The E' values (Fig. 9(a)) of the epoxy filled with a MERGO loading of 0.1, 0.25 and 0.5 phr are 10.63%, 44.21%, and 50.81% respectively, higher than that of neat epoxy within the glassy state (at 40 °C) and only a slight change is visible within the rubbery state (at 120 °C). The highest rate of improvement in E' at 0.25 phr MERGO loading is ascribed to the stiffness enhancement of MERGO in the hosting epoxy matrix. The lower rate of improvement in E' at 0.5 phr MERGO loading is caused by the change in the microstructure of E/MERGO nanocomposites as explained in earlier sections. E'' as a function of temperature also exhibits a similar trend to E' within the measured temperature scale. The maximum of E'', related to the motion of main chains of the epoxy networks at transition from the glassy state to the rubbery state for E/MERGO at 0.25 phr shift slightly to higher temperature compared with that (103 °C) of pure epoxy. This is because of the increased stiffness and constrained friction between polymer chains caused by the added MERGO [Fig. 9 (b)].

Fig. 9(c) shows the temperature dependent tan δ of cured pure epoxy and its MERGO composites. The tan δ is the ratio of E'' to E' and the peak of tan δ is often used to determine the glass transition temperature (Tg) of the material. As seen in Fig. 9(c), the Tg of E/MERGO 0.25 shifts slightly to a higher temperature (about 3–5 °C) compared to pure epoxy. This is because at optimum MERGO loading reinforcement of the polymer matrix is maximum and the flexibility of the epoxy matrix decreases. However there is no change in Tg for the nanocomposite with 0.5 phr MERGO loading. For composites with more MERGO, the reaction between MERGO and amine curing agent also should easily occur during the curing process. This interfacial reaction leads to strongest interfacial interactions with epoxy resin, on the other hand it can change the stoichiometry of epoxy/TETA and microstructure of E/MERGO nanocomposites. As a result, the MERGO highly influences the molecular dynamics and cross linking density of epoxy matrix, thereby increase the storage modulus and reducing the Tg of the composites. Similar kinds of results have been observed by various authors [15,37,38]. The height of the tan δ peak is observed to decrease with increasing MERGO percentage which shows lower damping, enhanced stiffness and good MERGO-epoxy interaction. It was reported that the lowering of tan δ values are an indicative of improvement in the interfacial reinforcement of the nanocomposites [39,40]. Since the height depression in tan δ peak has been correlated with the chain mobility, a quantitative estimation of volume fraction of these constrained regions has been done by Rao and Pochan [41]. Reduced chain mobility due to the physical and chemical bonding of the epoxy chain segments to the MERGO surface caused a height reduction of tan δ peak during dynamic mechanical deformation. However the decrease in cross link density might be the reason for the Tg to remain unaffected at high MERGO loading. Reduction of Tg with high contents of graphene with simultaneous reduction of tan δ was reported by Feng et al. [29].

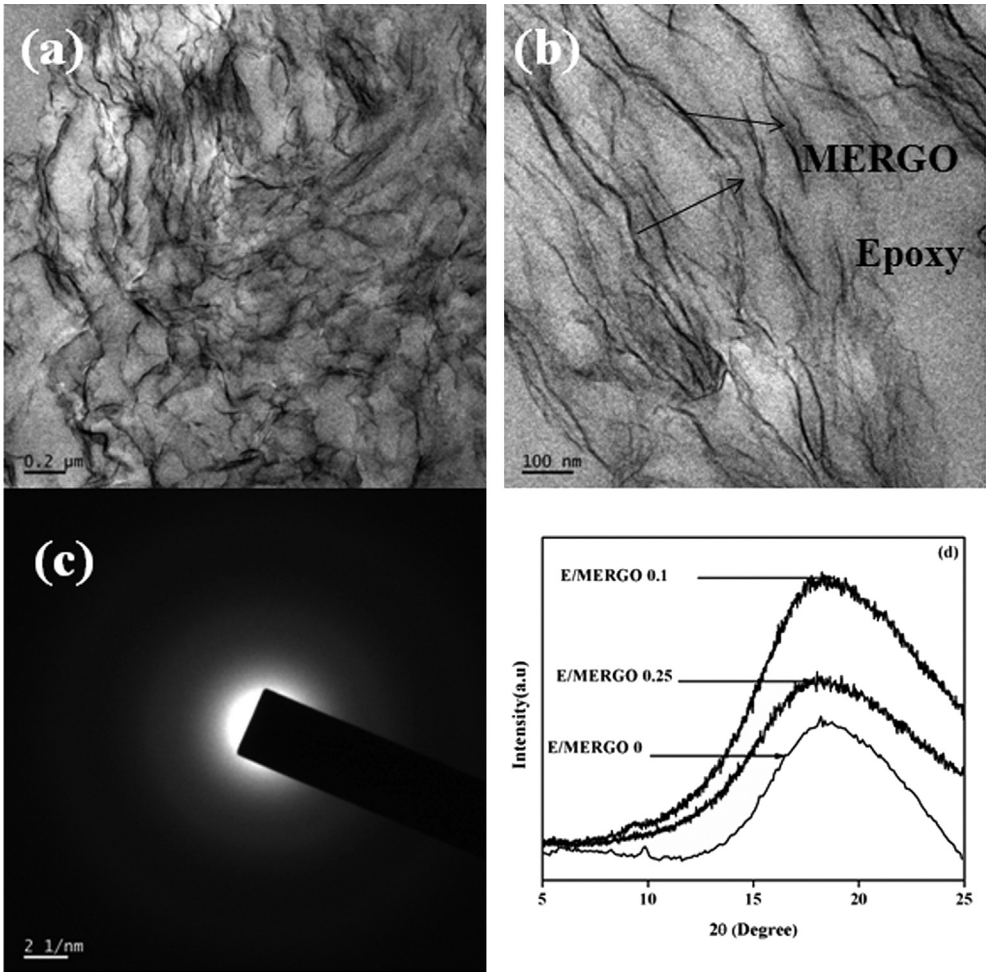

Fig. 8. (a & b) TEM image of E/MERGO nanocomposite with 0.25 phr MERGO loading at different magnification. (c) SAED pattern of E/MERGO at 0.25 phr loading. (d) XRD Pattern of pure epoxy and E/MERGO nanocomposites.

4.5. Dielectric properties

The excellent dielectric properties with a low and stable dielectric constant within a wide range of frequencies make epoxy a favorite of the electronic industry [42]. However their applications are limited due to their low electrical conductivity. Moreover the molecular motions or dynamics of nanocomposites in response to various applied field have an intense connection with the macroscopic properties [43]. Again the dielectric property measurements can be used as a tool to understand the charge transport mechanism in conducting polymer composites. Hence these properties should be investigated in the case of E/MERGO nanocomposites. Fig. 10(a, b, d & e) shows the AC conductivity, real permittivity (ε'), imaginary permittivity (ε'') and dielectric loss tangent ($\tan\delta = \varepsilon''/\varepsilon'$) as a function of the frequency (20 Hz–2 MHz) at room temperature for epoxy resin reinforced with different MERGO loadings. The AC conductivity is found to be increasing with increase in frequency [Fig. 10(a)]. Carbon materials such as graphene, CNTs, carbon fibers and carbon black are widely used to improve the electrical conductivity of composite materials [44–46].

The dependence of ε' as a function of frequency ranging from 20 Hz to 2 MHz at room temperature for E/MERGO is plotted in Fig. 10(b). The ε' for all samples exhibits a relatively large value at low frequency and remains nearly the same for a certain frequency range. The ε' for neat epoxy and 0.1 phr MERGO loaded epoxy composites exhibits lower dielectric performance. For the other concentrations, ε' increases with increase in loading and decreases with increase in frequency. At low frequencies, the dipole moments and the charge carriers can freely move within the E/MERGO nanocomposites and follow the varying electromagnetic field. While at high frequencies dipole and charge carriers become unable to follow variations of the applied electric field resulting in a decrease in ε'. In E/MERGO nanocomposites, the charges in conductive MERGO particles are easily delocalized, driven by the applied electric field. They accumulate at the interface of MERGO and epoxy insulator layers, leading to large scale polarization. As the MERGO content increases, Maxwell–Wagner (MW) polarization is significantly improved. Although the functional group present on the MERGO surface reduce the polarization process to some extent, the compatibility of MERGO/epoxy at the interface together with large surface area cause a 42% increase in ε' at 0.5 phr MERGO loading.

Fig. 10(c) refers dielectric constant at different frequency with the MERGO loading. Variation of ε' with MERGO loading is in agreement with Muradyan et al. [47]. Change in microstructure from fully exfoliated morphology of E/MERGO nanocomposites at lower loading to partially exfoliated or intercalated causes a decrease in interfacial polarization upto 2.5 phr. However with further loading, increase the number of intercalates, which decreases the thickness of dielectric spacers between conducting structures and increases the electrical capacitance. Moreover as the frequency of the applied electric field increases, gradually a situation arises, when dipoles present in the system can not reorient themselves fast enough to respond to applied field together with decreasing rate of interfacial polarization leads to a decrease in dielectric constant with increase in frequency.

The variation of ε'', the imaginary part of complex permittivity and tan δ of E/MERGO nanocomposites with frequency is presented in Fig. 10(d) and (e) respectively. E/MERGO nanocomposites exhibit an initial decrease which may be due to some kind of relaxation and

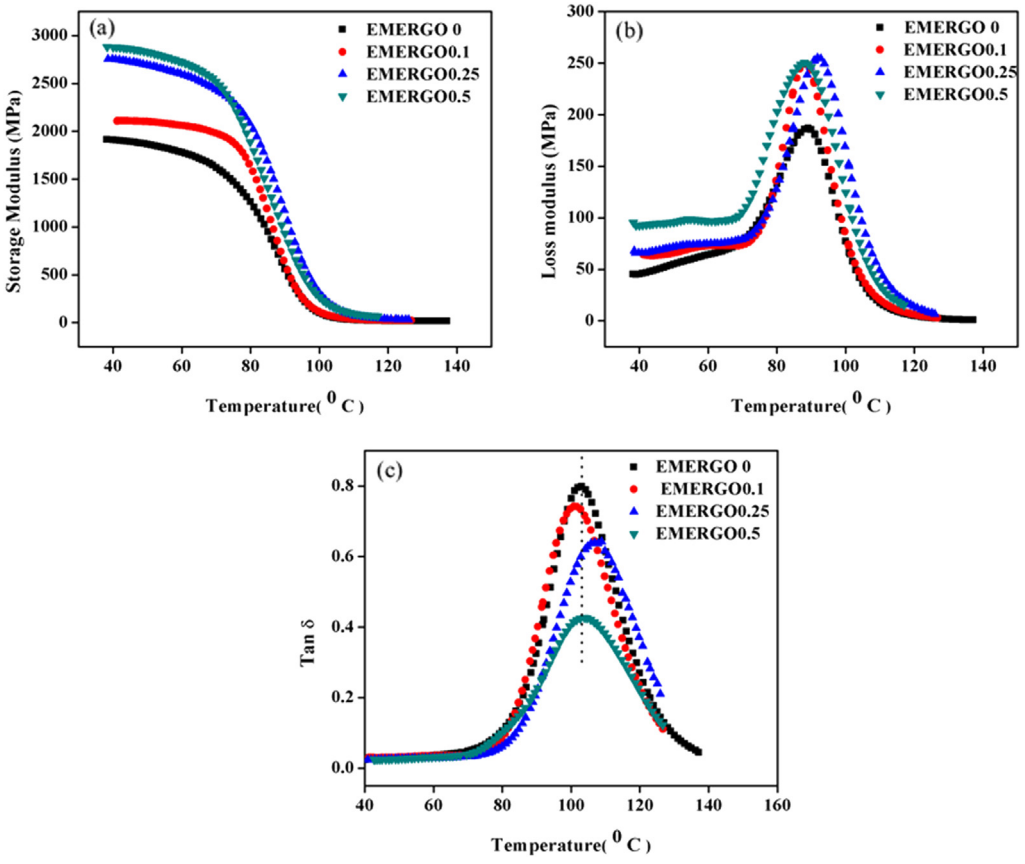

Fig. 9. Dynamic mechanical analysis, (a) storage modulus (E'), (b) loss modulus (E''), and (c) damping factor (tan δ) for the pure epoxy and E/MERGO nanocomposites.

then increase of these properties with frequency. The dielectric behavior of composites depends up on the type of matrix, method of preparation, molecular structure, particle size and crystal structure. Dielectric loss arises due to the localized motion of charge carriers.

The electrical percolation network of the cured samples is also analyzed by measuring DC electrical conductivity depicted in Fig. 10(f). As we know, a sharp increase in the electrical conductivity of composites can be expected only when a continuous conductive network is formed by conductive nanoparticles. Moreover the filler need not be in direct contact for current flow, rather conduction can takes place via tunneling between thin polymer layers surrounding the filler particles [48]. It is well known that conductivity of a conductor–insulator composite follows the critical phenomenon around the percolation threshold which can be described by a scaling law in the form of $\sigma \propto (p-p_c)^{\beta}$, where σ is the composite conductivity, p is the MERGO volume fraction, p_c is the percolation threshold and β is the critical exponent. The straight line graph from log–log plot of σ vs. $(p-p_c/p_c)$ illustrated in the inset of Fig. 10(f) with $p_c \sim 0.2696$ vol% (=0.5 phr) and $\beta = 1.001$, and a correlation factor of R^2 0.978 gives a good fit to the data. The magnitude of increase of electrical conductivity in E/MERGO nanocomposites is lower compared to pristine graphene epoxy nanocomposites [49]. The functionalization disturbs the crystalline graphitic structure by reducing the number of π electrons and generating sp^3 carbons, which do not cause such high electronic transport as π electrons in pristine graphene.

5. Conclusions

MERGO was synthesized from natural graphite through a simple, fast, and cost effective microwave exfoliation technique.

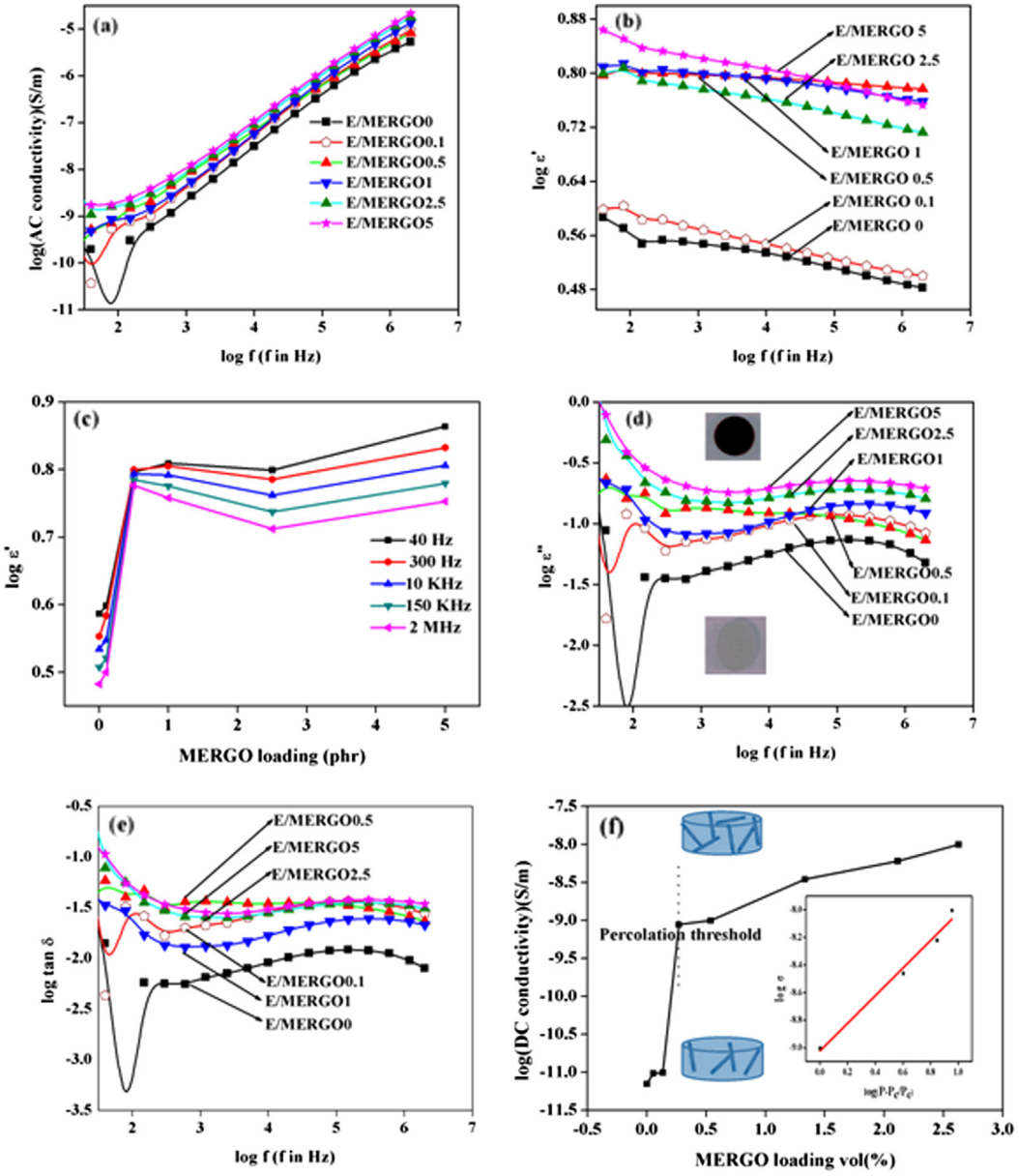

Fig. 10. Dielectric properties (a) AC conductivity, (b) Real permittivity (ε'), (c) Variation of real permittivity with MERGO loading, (d) Imaginary permittivity (ε'') [inset shows the samples for dielectric measurements] and (e) Dielectric loss tangent as a function of the frequency (20 Hz–2 MHz) at room temperature for pure epoxy and E/MERGO nanocomposites.(f) Variation of DC conductivity with MERGO loading [inset shows log–log plot of σ vs. $(p-p_c/p_c)$. Schematics of dispersion of MERGO in epoxy before (below) and at percolation (above) are also shown in inset].

Various techniques such as XRD, Raman, EDX, TGA, XPS, FTIR, C^{13} NMR, SEM, TEM and UV-vis were adopted to establish the occurrence of simultaneous reduction and exfoliation during microwave exfoliation. E/MERGO nanocomposites were fabricated by incorporating conductive filler MERGO into the epoxy matrix. Static mechanical, dynamic mechanical and dielectric properties of the epoxy resin reinforced with MERGO were conducted. XRD, SEM and TEM were done to analyze the quality and quantity of micro structural distribution of MERGO in the epoxy matrix. The E/MERGO nanocomposites with 0.25 phr MERGO loading showed an enhancement of 32% in tensile strength, 103% in impact strength and 85% in flexural strength compared to pure epoxy. The 0.25 phr MERGO sheets incorporated into the epoxy matrix effectively disturbed the development of crack growth and prevented crack propagation and lead to a significant increase in stress intensity factor K_{IC} upto 63%. Morphological characterization such as SEM and TEM were performed on the E/MERGO nanocomposites and correlated with their mechanical performance. The storage modulus ($E^{'}$) of E/MERGO nanocomposites was higher than that of neat epoxy within the glassy state. Tg of E/MERGO 0.25 shifts slightly to a higher temperature (about 3–5 °C). The E/MERGO nanocomposite attained an ac conductivity of 10^{-5} S/m and the dielectric constant was also remarkably increased. The combination of good processing properties with enhanced mechanical and dielectric properties makes MERGO great candidate to develop multifunctional polymer nanocomposites which has sought extensive application in Electromagnetic interference shielding (EMI), conductive adhesives and for thermal conductivity enhancement.

References

[1] Jeena JK, Narasimha Murthy HN, Rai KS, Krishna M, Sreejith M. Polym Plast Technol Eng 2010;49:1207–13.
[2] Moazzami GM, Sharif F. Express Polym Lett 2012;6:1017–31.
[3] Mildred Q, Ester V, Maurizio P. Acc Chem Res 2013;46:138–48.
[4] Geim AK, Novoselov KS. Nat Mater 2007;6:183–90.
[5] Liang-Xu D, Qiang C. Front Mater Sci China 2010;4(1):45–51.
[6] Veerappan M, Shen MC, Bih SL. Int J Electrochem Sci 2013;8:11641–60.
[7] Daniel RB, Erika GH, Ignacio MG. Macromolecules 2012;45:238–45.
[8] Brodie BC. Annales des Chimie et des Physique 1860;59:466.
[9] Staudenmaier L. Verfahren zur L, Graphitsaure DD, Deutschen BD, Gesellschaft C 1898;31:1481.
[10] Hummers WS, Offeman RE. J Am Chem Soc 1958;80:1339.
[11] Daniela CM, Dmitry V, Kosynkin, Jacob MB, Alexander S, Zhengzong S, et al. ACS Nano 2010;4:4806–14.
[12] Dorsa P, Sriya D, Ahmed THS, Fahmida I, Sanjoy B, Micah JG. ACS Nano 2012;6:8857–67.
[13] Yanwu Z, Shanthi M, Meryl DS, Aruna V, Richard DP, Rodney SR. Carbon 2010;48:2118–22.
[14] Li Y, Diyuan P, Shoubin CQ, Wang, Guangqin P, Wang T. Mater Des 2013;47:850–6.
[15] Chen Li, Songgang C, Kai L, Nanying N, Jian G, Qianfa L, et al. ACS Appl Mater Interfaces 2012;4:4398–404.
[16] Alamri H, Low IM, Alothman Z. Compos Part B 2012;43:2762–71.
[17] Park J, Jana SC. Polymer 2004;45:7673–9.
[18] Narteh AT, Hosur M, Triggs E, Peter Owuor P, Jelaani S. Polym Degrad Stab 2014;101:81–91.
[19] Gojny Florian H, Schulte K. Compos. Sci Technol 2004;64:2303–8.
[20] Vennerberg D, Rueger Z, Kessler MR. Polymer 2014;55:1854–65.
[21] Serra N, Maeder T, Ryser P. Sens Actuators A Phys 2012;186:198–202.
[22] Liang Q, Nyugen MT, Moon KS, Watkins K, Morato LT, Wong CP. J Electron Mater 2013;42:1114–21.
[23] Julia AK, Danielle RK, Ibrahim M, Greg MO. J Appl Polym Sci 2013;128:4217–23.
[24] Gallego MM, Bernal MM, Hernandez M, Verdejo R, Lopez-Manchado MA. Eur Polym J 2013;49:1347–53.
[25] Yang SY, Lin WN, Huang YLi, Tien HW, Wang JY, Ma CCM, et al. Carbon 2011;49:793–803.
[26] Zhang X, Alloul O, He Q, Zhu J, Verde MJ, Li Y, et al. Polymer 2013;54:3594–604.
[27] Zaman I, Phan TT, Kuan HC, Meng Q, Bao La LT, Luong LYO, et al. Polymer 2011;52:1603–11.
[28] Wang X, Xing W, Zhang P, Song L, Yang H, Hu Y. Compos Sci Technol 2012;72:737–43.
[29] Feng H, Wang X, Wu D. Ind Eng Chem Res 2013;52:10160–71.
[30] Ni Z, Wang Y, Yu T, Shen Z. Nano Res 2008;1:273–91.
[31] Joe Hodkiewicz. Thermo scientific Application note 51946.
[32] Guo Y, Chenlu B, Song L, yuan B, Hu Y. Ind Eng Chem Res 2011;50:7772–83.
[33] Liu J, Tang J, Goodling JJ. J Mater Chem 2012;22:12435–52.
[34] Shi WM, Li J, Jun BD, Sheng XZ. J Mater Sci 2013;48:156–61.
[35] Saw SWP, Mariatti M. J Mater Sci Mater Electron 2012;23:817–24.
[36] Li Z, Young RJ, Wang R, Yang F, Hao L, Jiao W, et al. Polymer 2013;54:5821.
[37] Wang L, Wang K, Chen L, Zhang Y, He C. Compos Part A 2006;37:1890–6.
[38] Ma PC, Kim JK, Tang BZ. Compos Sci Technol 2007;67:2965–72.
[39] Idicula M, Malhotra SK, Joseph K, Thomas S. Compos Sci Technol 2005;65:1077–87.
[40] Bindu P, Thomas S. J Phys Chem B 2013;117:12632–48.
[41] Rao YQ, Pochan JM. Macromolecules 2007;40:290–6.
[42] Sinh LH, Son BT, Trung NN, Lim DG, Shin SJ, Bae Y. React Funct Polym 2012;72:542.
[43] Sadasivuni KK, Ponnamma D, Thomas S, Grohens Y. Prog Polym Sci 2014;39:749–80.
[44] Kim H, Miura Y, Macosko CW. Chem Mater 2010;22:3441–50.
[45] Long YZ, Chen ZJ, Zhang XT, Zhang J, Liu ZF. Appl Phys Lett 2004;85:1796–8.
[46] Hu N, Masuda Z, Yan C, Yamamoto G, Fukunaga H, Hashida T. Nanotechnology 2008;19:215701.
[47] Muradyan VE, Sokolov EA, Piven NP, Babenko SD, Allayarov SR. Tech Phys Lett 2010;36(12):1115–7.
[48] Potts JR, Dreyer DR, Bielawski CW, Ruoff RS. Polymer 2011;52:5–25.
[49] Lianga J, Wanga Y, Huanga Y, Maa Y, Liua Z, Caib J, et al. Carbon 2009;47:922–5.